



HAL
open science

Three-Dimensional Microstructure of a Polymer-Dispersed Liquid Crystal Observed by Transmission Electron Microscopy

Jean Pierron, Valérie Tournier-Lasserve, Pierre Sopena, Alain Boudet, Pierre Sixou, Michel Mitov

► **To cite this version:**

Jean Pierron, Valérie Tournier-Lasserve, Pierre Sopena, Alain Boudet, Pierre Sixou, et al.. Three-Dimensional Microstructure of a Polymer-Dispersed Liquid Crystal Observed by Transmission Electron Microscopy. *Journal de Physique II*, 1995, 5 (11), pp.1635-1647. 10.1051/jp2:1995204 . jpa-00248260

HAL Id: jpa-00248260

<https://hal.science/jpa-00248260>

Submitted on 4 Feb 2008

HAL is a multi-disciplinary open access archive for the deposit and dissemination of scientific research documents, whether they are published or not. The documents may come from teaching and research institutions in France or abroad, or from public or private research centers.

L'archive ouverte pluridisciplinaire **HAL**, est destinée au dépôt et à la diffusion de documents scientifiques de niveau recherche, publiés ou non, émanant des établissements d'enseignement et de recherche français ou étrangers, des laboratoires publics ou privés.

Classification

Physics Abstracts

61.16-d — 61.30-v

Three-Dimensional Microstructure of a Polymer-Dispersed Liquid Crystal Observed by Transmission Electron Microscopy

Jean Pierron⁽¹⁾, Valérie Tournier-Lasserre⁽¹⁾, Pierre Sopena⁽¹⁾, Alain Boudet⁽¹⁾, Pierre Sixou⁽²⁾ and Michel Mitov⁽²⁾

⁽¹⁾ CEMES-LOE, CNRS, BP 4347, 31055 Toulouse Cedex, France

⁽²⁾ Laboratoire de Physique de la Matière Condensée(*), Parc Valrose, 06108 Nice Cedex 2, France

(Received 3 April 1995, revised 21 July 1995, accepted 11 August 1995)

Abstract. — A film consisting of an amorphous photo-crosslinkable polymer matrix and a dispersion of micronclusions of a cholesteric polymer was investigated by transmission electron microscopy (TEM). The polymerization procedure of the blend provides a composite with many small nodules of spherical or ellipsoidal shapes, with sizes between 0.4 and 6 μm . The cholesteric stratification is well evidenced in transmission electron microscopy by dark lines due to diffraction contrast. The 3D organization was reconstructed by the observation of successive ultramicrotomed sections. Six types of nodules were distinguished according to the number of defects (foci or disclination lines), among which only three had already been observed and theoretically calculated. The confined geometry inherent in the size of the nodules, close to the cholesteric pitch, is responsible of these unexpected structures. In these conditions, the surface forces are in tight competition with the cholesteric elastic forces

1. Introduction

A microcomposite film, consisting of an amorphous photo-crosslinkable polymer matrix and a dispersion of micronclusions of a cholesteric polymer, was investigated by transmission electron microscopy (TEM). The aim of this study was to evidence the shapes, the sizes and the distribution of the micronclusions. We describe the inner structure of the cholesteric microdroplets with the aid of TEM and compare it with the structure of the same polymer alone, already studied in a previous paper [1]. From this comparison, some considerations can be drawn concerning the competition between the elastic forces and the surface energies.

Microcomposite films including liquid crystals are of great interest because of their applications in numerous fields: large-area displays, electrically controlled glasses, light valves [2–5]. In these films with a closed or open porosity according to the proportion of the liquid crystal present [6], the properties of the liquid crystals, in particular their electrooptic response, are

(*) UA CNRS 190.

modified by their confinement inside the microinclusions or in the network cells. It is therefore very important to determine the geometry of the liquid crystal dispersed in the matrix and the distribution of the molecule director. Light microscopy is often unable to provide such information because of its limited resolution, so that electron microscopy must be used. However, only very thin slices of specimens, sectioned by ultramicrotomy, can be observed in TEM. During this process the small fluid molecular liquid crystal is lost. In this study, this does not happen because the liquid crystal is a polymer, solid at room temperature.

2. Specimens

The material studied is a blend of an amorphous polymer and a cholesteric side chain copolysiloxane. The copolysiloxane consists of a cyclic main chain on which two types of side moieties are attached by a spacer: n biphenyl moieties with a nematic character and m chiral cholesteryl moieties that give the cholesteric structure (Fig. 1). As the ratio $m/(m+n)$ of the chiral moieties increases, the cholesteric pitch P and the reflected light wavelength decrease. The number of siloxane units $m+n$ of the polymer studied in this work varies between 3 and 7 with 5 being the most common value. The ratio $m/(m+n)$ is 0.5, the pitch $0.29 \mu\text{m}$ and the light is reflected in the blue range (Tab. I). This cholesteric polymer was synthesized by Kreuzer [7-9].

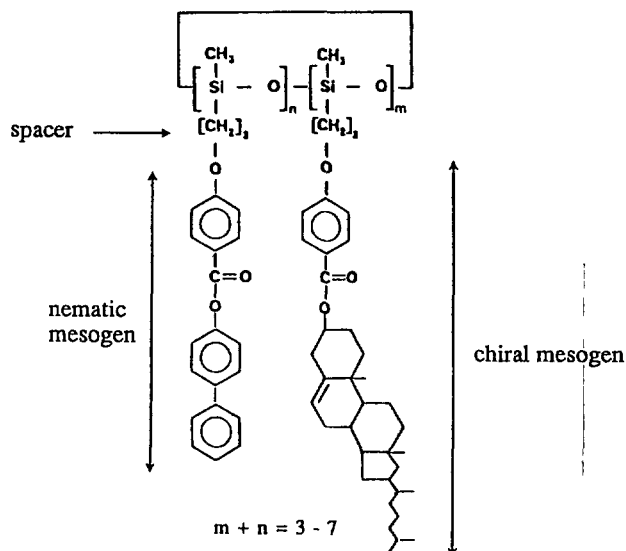


Fig 1 — Scheme of the copolysiloxane formula

The initial solution of the composite contains 30% of this cholesteric and 70% of an epoxy prepolymer. It is heated at $150 \text{ }^\circ\text{C}$ between two glass slides, crosslinked by exposure to UV rays, and cooled down to room temperature in the form of a film 20 micrometers thick. During this process a demixion of the liquid crystal occurs and gives rise to the formation of nodules included in the epoxy matrix.

Table I. — *Some physical properties of the cyclic copolysiloxane.*

	silicone blue
$m/(m + n)$ ratio	0.5
cholesteric pitch /nm	290
reflexion wavelength /nm	450
glass transition temperature /°C	40/50
clearing temperature /°C	180/210
processing temperature /°C	160

3. Transmission Electron Microscopy

Very few studies have been carried out on this type of composite in TEM, partly because of the fluidity of the liquid crystals, and partly because of the amorphization of the liquid crystal during electron radiation.

This copolysiloxane has already been studied by scanning electron microscopy [10], atomic force microscopy [10] and TEM [1, 10]. In TEM, the cholesteric structure is evidenced by alternate dark and bright lines with a periodicity equal to half the cholesteric pitch. Two contrast mechanisms were identified [1]. a diffraction contrast on specimens not damaged by the electron beam, then a thickness contrast develops as radiation proceeds.

A small piece of the composite film was embedded in an epoxy resin then sectioned with an ultramicrotome using a diamond knife. The thickness of the slices is about 125 nm. The slices were then deposited on carbon coated grids and observed in TEM with a Jeol 200 CX microscope or a Philips CM 20 microscope. The micrographs exhibiting diffraction contrast were recorded in minimum dose conditions, on areas that had not previously been exposed to the beam. After exposure, we ensured that the diffraction pattern was still a cholesteric one and not altered towards an amorphous pattern.

Other sections about 3 μm thick were also prepared for observation in light microscopy between crossed polars.

4. Shape and Distribution of the Microinclusions

In light microscopy between crossed polars, the microinclusions, visible since they are birefringent, have the shape of disks or ellipses (Fig. 2). The elliptic shape is not due to the compression by the knife during ultramicrotomy since the orientations of the axes are random and not correlated with the cutting direction. The nodules are distributed homogeneously and dispersed randomly. Many pictures were taken (Fig. 2), digitized, then analysed by computer using the "IMAGE" software. About 1500 nodules were recorded and analysed.

A histogram of the diameter lengths D of the nodules is presented in Figure 3. They fall between 0.4 and 6 μm . In the case of the ellipses, the size D is taken as the length of the long axis. The most frequent nodules are about 1 μm in diameter and the large ones (over 3 μm) are very seldom seen. Some of the large nodules result from the coalescence of several small ones. There are about 88% discs and 12% ellipses.

Since the disks and ellipses in the observed slices are sections of spheres or ellipsoids seen in a horizontal plane that is rarely their equatorial plane, the large equatorial circle of the thicker nodules may not be included in the slice, so that the real size of the nodule may be larger and the real histogram should be slightly shifted towards the larger sizes.

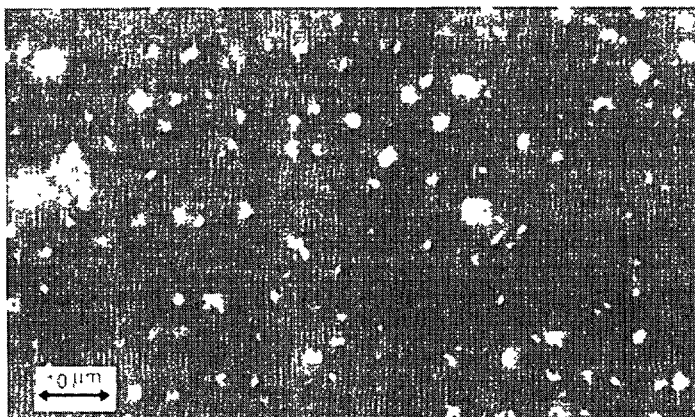


Fig. 2. — Dispersion of liquid crystal nodules. Light microscopy (the windy lines are corrugations of the matrix due to ultramicrotomy).

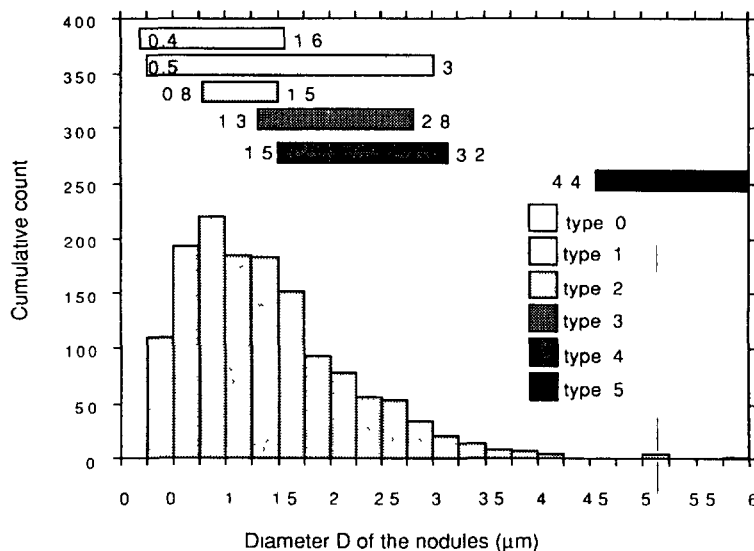


Fig. 3 — Histogram of the size D of the nodules, from a set of light microscopy micrographs. At the top, the range of the sizes of the 6 types has been reported according to TEM observations.

In this size range of the nodules, no internal structure is visible in light microscopy. Transmission electron microscopy (TEM) has been used to obtain a better resolution.

5. Cholesteric Three-Dimensional Structure of the Nodules

The same disks and ellipses are clearly recognizable in bright-field micrographs (Fig 4). To reveal the relative locations of the constituents in a blend of polymers, researchers usually add a stain in order to darken one of the constituents with respect to the others. Sometimes, this is not really useful and can provoke artefacts. In the absence of any stain, the polysiloxane studied here appear slightly darker than the matrix, so that images can be recorded.

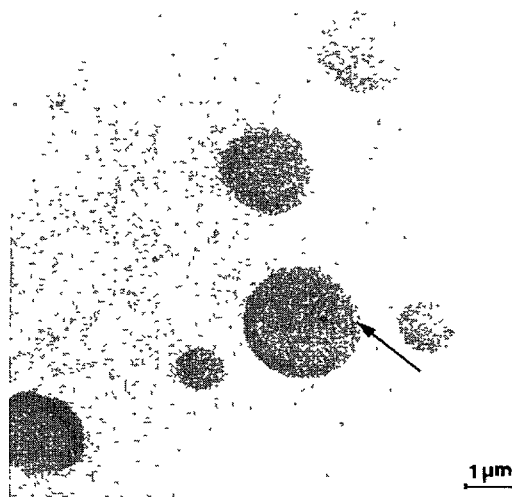


Fig 4. — Dispersion of some liquid crystal nodules, where the cholesteric stratification is visible. The arrow points to a disclination. Transmission electron microscopy, bright field

Furthermore, thanks to this absence of stain, another weaker contrast can be seen. The internal cholesteric stratification comes out as alternate bright/dark lines, as described in reference [1] for the pure polysiloxane. In that paper, we showed that the periodicity of the lines was equal to the periodicity of the cholesteric structure (half pitch $P/2$). The cholesteric axis is perpendicular to the lines. We demonstrated that the lines are due to diffraction contrast when the specimen is still undamaged by the electron beam. In the dark lines, the side chains lie in the substrate plane, and are parallel to the lines. The dark lines are therefore a partial representation of the director field lines.

During the observation of the nodules, the specimen is damaged by the electron beam and the contrast of the lines in the nodules increases. In [1], the increase of the contrast in microtomed specimens was explained as a progressive etching of the surface, leading to a periodic relief of the surface. As in reference [10], we imaged and measured this relief on the pure polymer [11].

In the nodules, we measured the periodicity in areas where the lines are straight and found an average value about 10% lower than in the non confined polymer. Although the lines are sometimes straight, they are most often curved into portions of concentric circles or ellipses, around a centre (focus). When the curvature is weak, this focus lies geometrically out of the nodule. When the focus is visible in the nodule, the curvature is strong and gives rise to a disclination (Fig. 4). As in this figure, the central line of the disclination is most often white indicating that the molecules are perpendicular to the section (λ disclinations) [1]. Sometimes, τ disclinations are also visible. In reference [1], we found that in very thin layers on the contrary, τ disclinations occurred more frequently than λ disclinations. We attributed it to the mode of preparation and the influence of the surfaces. The predominance of the λ disclinations in the bulk specimens was predicted by energy calculations [12].

Different types of figures of these lines are present, which we could classify according to the number of foci in the nodule. We identified six types of figures in the two-dimensional plane of the section (Figs. 5a-f). Types 0 to 4 have respectively 0 to 4 foci, and they appear in the proportion of 17%, 35%, 28%, 13% and 7%. Type 5 is rare and displays a fingerprint texture.

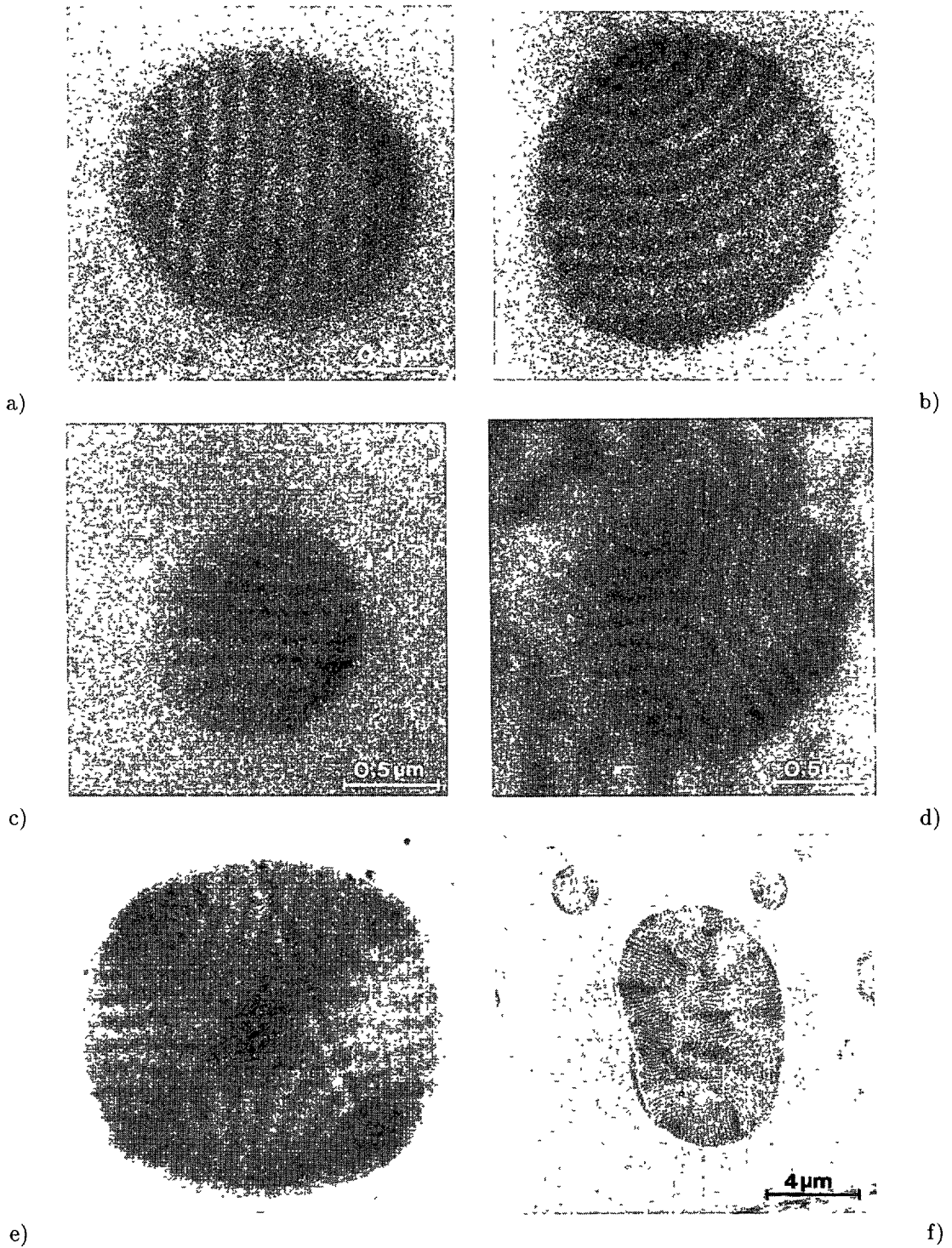


Fig. 5. — Examples of the different types of nodules classified according to their number of foci: 5a) type 0; 5b) type 1, 5c) type 2, 5d) type 3, 5e) type 4, 5f) type 5.

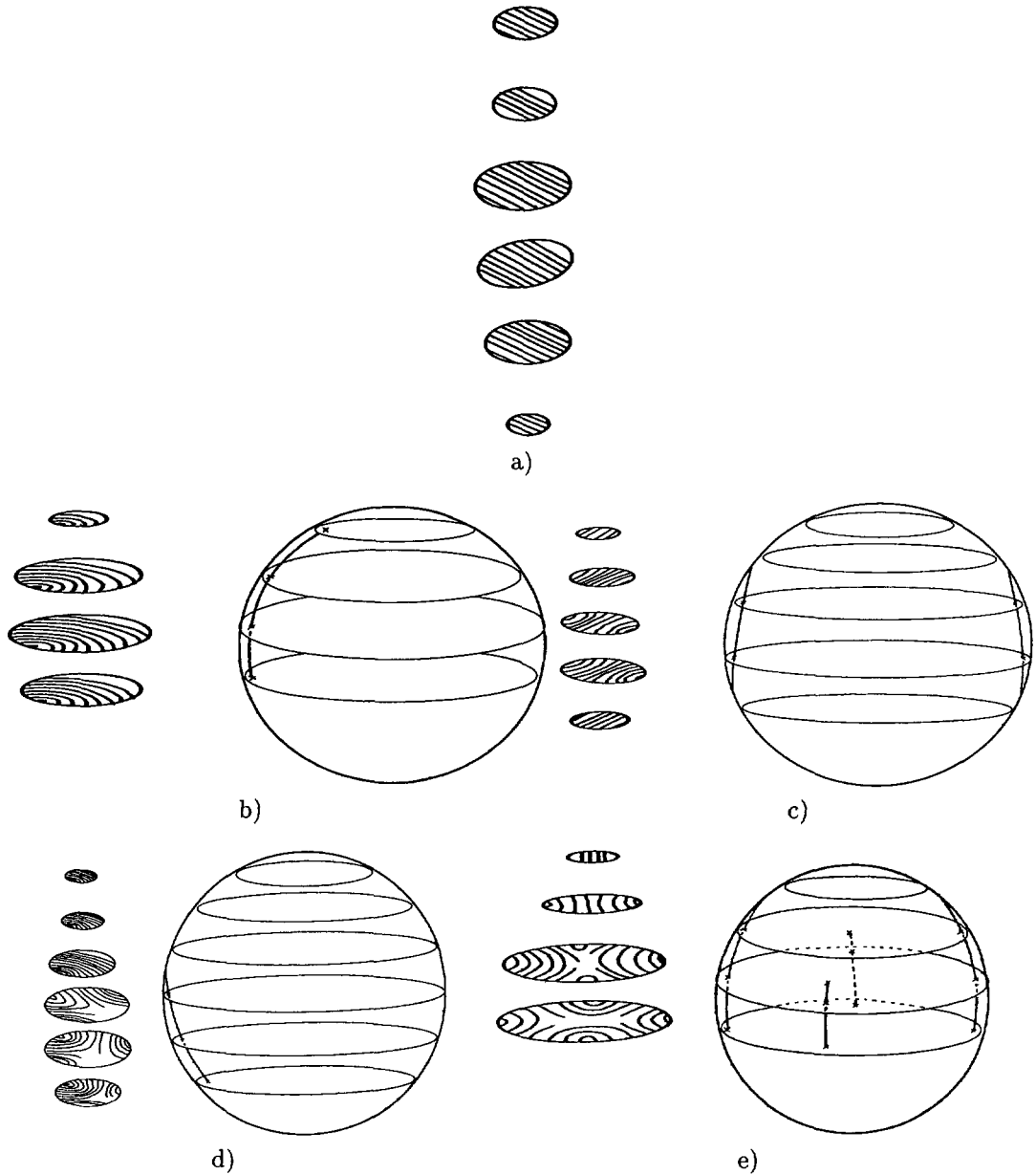


Fig 6. — Three-dimensional reconstruction of a few nodules. On the left, the overlay patterns of the dark lines in successive sections have been superposed, and reduced in one dimension to create the illusion of a perspective. On the right, sketch of the disclination lines joining the foci. 6a) Type 0; 6b) type 1, 6c) type 2, 6d) type 3; 6e) type 4

A difficult question is how these figures are organized in three dimensions. For some nodules, we succeeded in obtaining successive sections of the same nodule, so that we could reconstruct the geometry of the lines in three dimensions (Fig. 6). It must be kept in mind that the lines are not areas physically differentiated from the surroundings, but the locus of points at which

the molecules are perpendicular to the electron beam and parallel to one another, that is to say they are isocline contours.

5.1. ISOCLINE SURFACES IN TYPE 0-NODULES. — In the type 0-nodule, no focus is found. The dark lines in the ellipses are straight (Fig. 5a). Their number varies from 2 to 9. The length of the long axis of the nodules lies between 0.4 and 1.6 μm , and the distances between the lines between 100 and 130 nm. The nodule thickness was estimated by the number of successive sections of the same nodule (3 to 6), and the mean thickness of each section controlled by the ultramicrotome ($\sim 0.125 \mu\text{m}$). The results (0.3 to 0.7 μm) have shown that this thickness was lower or higher than the long axis in the section by up to 25%.

We tried to find out how the dark lines are related from one section to the next (Fig. 6a). The relative orientations of the sections were determined by the knife scratches. If we join the corresponding lines from one section to the next to form a continuous surface, we construct an isocline surface. In the type 0-nodules, the isocline surfaces are quasi-parallel planes (Fig. 7). When the nodules are sectioned perpendicularly to these planes (Fig. 7a), all of the sections

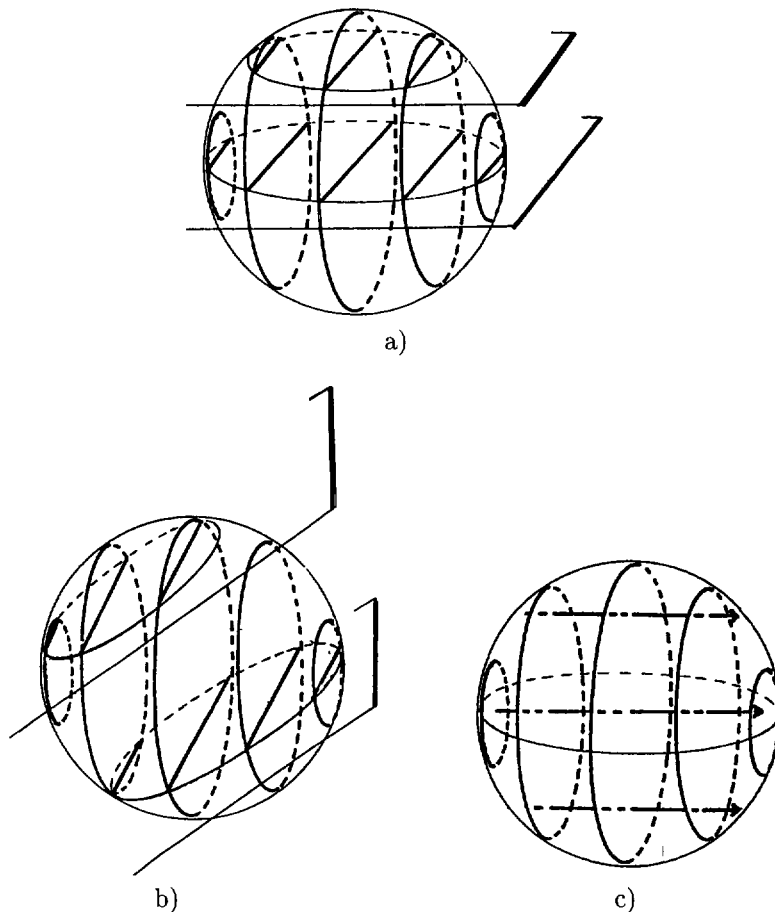


Fig. 7. — Construction of the isocline surfaces in a type 0-nodule: a) section by two horizontal planes; b) section by two oblique planes; c) cholesteric axis field lines.

exhibit the same symmetry. The central line remains the same. When passing from a disk at the end to the equatorial disk, two or an even number of supplementary lines appear. When the nodules are sectioned obliquely (Fig. 7b), the upper and lower lines are no longer superposed. Only one supplementary line appears in the next larger section. These two cases were observed so that it seems that the nodules are randomly oriented in the specimen.

The cholesteric axis field lines may be drawn since they are perpendicular to the isocline surface (Fig. 7c). It is clear that the cholesteric axis, keeping the same orientation in the whole volume of the nodule, does not adopt the spherical or elliptical symmetry of the external boundary. Consequently, the orientation of the molecules close to the surface is alternatively parallel and perpendicular to the boundary.

5.2. TYPE 1-NODULES. — In these nodules, one focus is found (Fig. 5b). The lines are weakly bent, the curvature is more pronounced around the focus. The diameter D varies between 0.5 and 3 μm with 4 to 19 lines. About four successive sections could be made in these nodules.

Reconstruction of the isocline surfaces through the sections shows surfaces with a slight curvature that increases close to the focus where they are bent like cups (Fig. 6b). The line joining the foci on the different levels is a disclination line (in Fig. 6b, a τ^+ disclination).

5.3. TYPE 2-NODULES. — Type 2-nodules contain two foci (Fig. 5c). They are located on the opposite extremities of a diameter in the disks, and of the long axis in the ellipses. Sometimes, one of the foci lies far outside the boundary so that the lines are weakly curved and the nodule is intermediate between the type 1 and the type 2. Their sizes vary between 0.8 μm and 1.5 μm , with 7 to 16 lines. Three to five successive sections could be achieved.

The figures of the successive sections can easily be superposed to construct the isocline surface (Fig. 6c). The foci are present in the larger section (equatorial) and progressively vanish in the lower and upper sections which are type 0-like. On the side where the foci lie inside the section, a disclination line joining these foci on the different levels can be drawn (here λ^+ disclinations). It emerges onto the surface at an intermediate level.

A sketch of the isocline surface is represented in Figure 8. It is seen that the cholesteric stratification tends to be perpendicular to the boundary (or the cholesteric axis parallel to it). It indicates an effect of the surface. This is an important difference with the zero-type nodules which is discussed in Section 6.

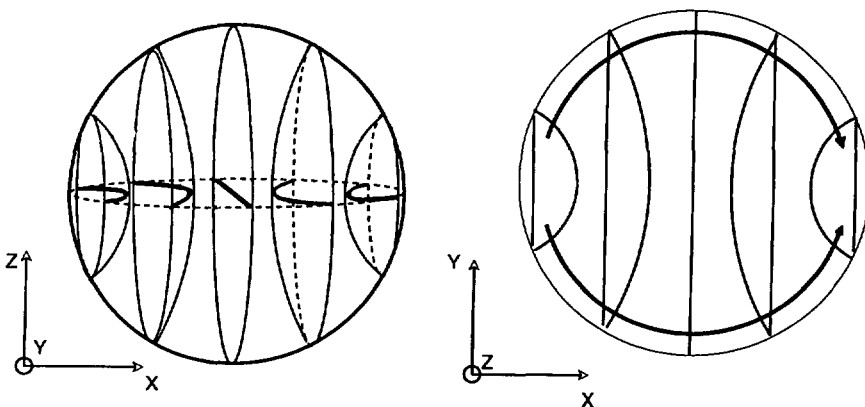


Fig. 8 — Construction of the isocline surfaces and cholesteric axis field lines in a type 2-nodule

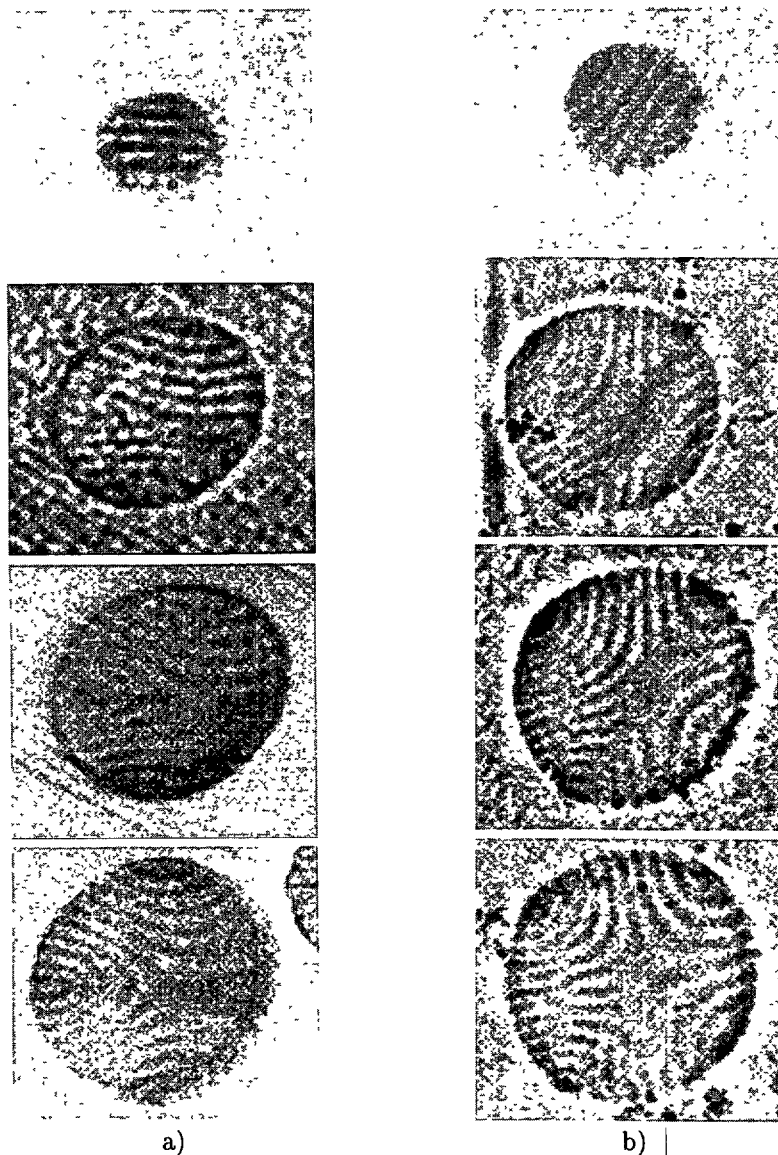


Fig. 9. — Sequences of micrographs of successive sections. Contrast enhancement by image processing. 9a) Type 3-nodule; 9b) type 4-nodule.

5.4. TYPE 3-NODULES. — The three foci of these nodules are often at 120° to one another (Fig. 5d), but in some cases, the angles depart greatly from this value. The diameter D varies from 1.3 to 2.8 μm , larger than for types 1 and most of types 2. Therefore, the number of foci seems to increase with the size of the nodule.

Figure 9a shows a sequence of successive sections of one nodule. The third focus is present only in the equatorial sections (Fig. 6d). The upper ones resemble type 1-sections, since only one focus is left and inside the nodule, a transition between type 1 and type 3 occurs. On the side where the foci lie inside the section, a disclination line can be drawn by joining these foci

on the different levels (λ^+ disclination). It emerges onto the surface at an intermediate level as in type 2-nodules. The isocline surfaces are more complicated. At the centre of the equatorial section, a λ^- disclination is visible (Fig. 5d).

5.5. TYPE 4-NODULES. — These nodules are still larger (1.5 to 3.2 μm). The four foci of these nodules are often at 90° to one another (Fig. 5e). In some cases, two of the foci are at opposite ends of a diameter of the disk and the other two are anywhere on the boundary.

Superposed sections (Figs. 6e and 9b) show that although four foci are present in the equatorial section only two are left in the upper sections, and none in the uppermost one. There is a transition between type 0, type 2 and type 4 inside this nodule. Four λ^+ disclination lines can be drawn, they emerge at intermediate levels. In the equatorial plane, the periodicity of the alternate lines increases towards the centre, while the curvature decreases (Fig. 9b). The isocline surfaces seem to be deformed, maybe in the form of a horse saddle. Like in type-2 and 3 nodules, the cholesteric axis tends to be parallel to the boundary.

5.6. TYPE 5-NODULE. — This type has no focus and its configuration is quite different from the others. It could correspond to the coalescence of two or several droplets. As it is still larger than the others, the fingerprint texture that was observed in the pure polymer [1] is again visible here (Fig. 5f). The external boundaries have no longer influence on the general organization of the texture.

6. Discussion and Conclusion

The shapes of the nodules result from the demixtion during polymerization. The cholesteric and the polymer matrix tend to segregate and the sphere is the volume in which they have the smallest common surface. The inner structure of the nodules depends on the balance between the internal elastic forces (due to the deformation of a regular cholesteric configuration) and the boundary forces. This balance is strongly related to the confinement ratio, ratio of the size D of the nodule over the cholesteric pitch P .

Types 1 to 4 represent the size where the two forces are equivalent. For these small ratios ($D/P = 1.7$ to 10 , or $D = 0.5$ to $3 \mu\text{m}$), the boundary forces have a strong relative part. The black lines are mostly perpendicular to the boundary surface (Fig. 5d for instance). It seems then that the surface forces impose the cholesteric axis to be parallel to the boundary in competition with the elastic forces which limit the deformation. The nature of the anchorage due to surface forces cannot be precised. They are of electric character and have been discussed elsewhere in the case of the cholesteric sandwiched between two glass slides [13].

For larger diameters, the boundary influence becomes limited to a small area of the nodule, so that the texture is ruled by the elastic forces and takes configurations similar to that of the cholesteric alone (fingerprint). On the opposite, in type 0-nodules which are very small, the boundary forces are strong, but they cannot impose the spherical symmetry of the surface in the volume. This can be explained because the elastic forces are still stronger on short distances and the cholesteric stratification cannot be easily bent on this reduced scale.

On an experimental point of view, cholesteric microdroplets have been observed since long by light microscopy [14, 15], as well as in emulsions of chiral nematics [16, 17], biological polymers [16], and polymer dispersed liquid crystals [18–20]. In these papers, expressed with the terms of our classification, type 0, 1 and 2 have been observed, but not types 3, 4 and 5. Type 0 has been more often observed in the small droplets, with $D/P \approx 1$ [18, 19].

On a theoretical point of view, minimization of the free energy in the tangential conditions leads to models of droplets [21, 22] with a planar configuration – corresponding to our type

0-nodule – or with a diametral defect, or a radial defect (which is equivalent to the model by Frank [23] and Price [24]). However the stability of these models was appreciated only for large droplets when $D/P \gg 1$ and in the tangential boundary conditions. When D/P is small, these calculations indicate that the planar structure is expected to be the more stable [18,21]. Models corresponding to our types 3 and 4 have never been envisaged.

Observations [25–27] and calculations [28,29] have also been performed in nematic droplets. In small droplets, they lead to the conclusions that a bipolar structure is the most stable for the tangential conditions, and an axial structure for normal conditions [28].

All these calculations cannot account for our observations which are made in the case where $D/P = 1$ to 10. Nevertheless, they are in accordance with them for the types 0, 1 and 2. For example, the planar structure is in accordance with our type 0 nodule, and this suggests that the boundary conditions of this nodule are tangential. On the contrary types 3, 4 and 5 had not been observed previously, nor predicted. From our observations, they correspond to boundary conditions where the cholesteric axis is parallel to the surface, and the molecules alternatively tangential and perpendicular to it. No model has never been calculated with these conditions. However, a small transition zone where the molecules pass from a tangential orientation to an alternate orientation is possible, although we could not detect such a zone in TEM.

The conclusion is that the polymerization procedure of the blend provides a composite with many small nodules of spherical or ellipsoidal shapes, with a size between 0.4 and 6 μm . The cholesteric stratification is well evidenced in transmission electron microscopy by dark lines due to electron diffraction contrast. Their three-dimensional organization was reconstructed by the observation of successive sections. Six types of nodules can be distinguished according to the number of defects (foci or disclination lines, really seen in the nodule, or virtual out of it), among which only three had already been observed and theoretically calculated. We think that the confined geometry inherent to the size of the nodules, close to the cholesteric pitch, is responsible for these unexpected structures. In these conditions, the surface forces are in tight competition with the elastic forces.

References

- [1] Pierron J., Boudet A., Sopéna P., Mitov M. and Sixou P., *Liquid Crystals* (1995) in press.
- [2] Ferguson J., *SID Dig. Tech. Pap.* **16** (1985) 68
- [3] Doane J.W., West J., Zumer S. and Blinc R., *Proc. SPIE* 958 (1988) 94
- [4] Macknick A.B., Jones P. and White L., *Proc. SPIE* 1080 (1989) 169.
- [5] Doane J.W., *Liquid Crystals. Applications and Uses*, Vol. 1, B. Bahadur, Ed. (World Scientific, 1990) pp 361-395.
- [6] Hikmet R., *Adv Mater.* **4** (1992) 679-683
- [7] Kreuzer F.H., *Proceedings 11. Freiburger Arbeitstatung Flussigkristalle* 5 (1981).
- [8] Kreuzer F.H., Gawhary M., Winkler R. and Finkelmann H., 981, EP 0060335.
- [9] Kreuzer F.H., Andrejewski D., Haas W., Haberle N., Riepl G. and Spes P., *Mol. Cryst. Liq. Cryst.* **199** (1991) 345-378
- [10] Bunning T.J., Vezie D.L., Lloyd P.F., Haaland N.D., Thomas E.L. and Adams W.W., *Liq. Crystals* **16** (1994) 769-781.
- [11] Pierron J., Tournier-Lasserve V., Boudet A. and Sopéna P., *Microscopy, Microanalysis, Microstructures in preparation.*
- [12] Kleman M., *Points, Parois, Lignes Tome 1* (Les Editions de Physique, 1977).

- [13] Mitov M and Sixou P., *Physica B* in press
- [14] Candau S., Le Roy P. and Debeauvais F, *Mol. Cryst Liq. Cryst* **23** (1973) 283-297.
- [15] Robinson C, Ward J C and Beevers R.B., *Disc Faraday Soc.* **25** (1958) 29.
- [16] Bouhgand Y. and Livolant F., *J Phys France* **45** (1984) 1899-1923.
- [17] Kurik M V and Lavrentovich O.D., *Mol. Cryst Liq Cryst.* **72** (1982) 239-246.
- [18] Yang D K and Crooker P.P., *Liq. Cryst* **9** (1991) 245-251.
- [19] Yang D K. and Crooker P.P., SPIE 1257 (1990) 60-67.
- [20] Kitzerow H S , *Liq. Cryst* **16** (1994) 1-31.
- [21] Bezic J and Zumer S , *Liq Cryst.* **11** (1992) 593-619
- [22] Zumer S , Kralj S. and Bezic J., *Mol Cryst Liq Cryst.* **212** (1992) 163-172
- [23] Frank F.C , *Disc. Faraday Soc* **25** (1958) 1.
- [24] Price F P , *J Polym Sci* **39** (1959) 139.
- [25] Ding J., Zhu J and Yang Y , *Jpn J. Appl. Phys* **33** (1994) 1400-1406
- [26] Ding J and Yang Y , *Jpn J Appl Phys* **31** (1992) 2837-2845.
- [27] Draicz P , *Mol Cryst Liq Cryst* **154** (1988) 289-306.
- [28] Dubois-Violette E and Parodi O , *J Phys Colloq France* **30** (1969) C4-57-64.
- [29] Williams R.D , *J Phys A* **19** (1986) 3211-3222